Ultralow density plume measurements using a helium mass spectrometer

Y. Jafry
Department of Aero/Astro, Stanford University, Stanford, California 94305-4085

J. Vanden Beukel
Lockheed Missiles and Space Company, Sunnyvale, California 94089

(Received 9 August 1991; accepted 23 September 1991)

Gravity Probe-B and the Satellite Test of the Equivalence Principle are two proposed experiments in basic physics which will utilize *drag-free* satellites equipped with proportional helium thrusters. In order to calibrate the thrust systems for precise *aeronomic* measurements, it is necessary to model the effects of thruster plume impingement. Conventional plume models are invalid, owing to the high degree of rarefaction in the nozzles (Kn = 0.01–1.1). An experiment was devised to measure the plume angular mass flux distribution using a helium mass spectrometer. The results suggest that the plume shapes are unchanged with mass flows around the nominal, and are generally wider than for conventional spacecraft control jets. A narrowing effect was observed at very low mass flows, in qualitative agreement with Monte Carlo results from the literature. The continuum model for the plume was found to be surprisingly accurate at nominal mass flows, and the inverse-square law was demonstrated to be a valid description of the far-field radial density profile.

I. INTRODUCTION

A. Gravity Probe-B and the Satellite Test of the Equivalence Principle

Gravity Probe-B (GP-B) and the Satellite Test of the Equivalence Principle (STEP) are two Stanford University proposals for space experiments in basic physics. GP-B will investigate two predictions from Einstein's Theory of General Relativity by monitoring the relativistic precession of an earth-orbiting gyroscope. STEP will attempt to verify the Equivalence Principle to unprecedented accuracy by looking for any difference in the acceleration of two unlike masses in the earth's gravity field, to one part in $10.^{17}$

Both experiment payloads will be cryogenically cooled with liquid helium. The boil-off helium gas will be vented through proportional thrusters for *drag-free* and attitude control of the host spacecraft. By monitoring the thruster activity, it will be possible to deduce the atmospheric drag, from which density and wind variations may be inferred to unprecedented spacial and temporal resolution. The accuracy of these *aeronomic* measurements will be limited by the levels to which the thruster systems can be calibrated. One of the largest sources of uncertainty will be the impingement of the thruster plume gas on the spacecraft surfaces, so it is desirable to model these effects.

B. Conventional plume models

Conventionally, thruster plume calculations are performed based on the assumption of continuum flow in the thruster nozzle. Application of Prandtl–Meyer theory at the nozzle lip can be used to approximate the expansion of the isentropic core, yielding an expression for the angular variation in density across the plume. In the far-field, the nozzle appears as a point source with gas emanating radially at a constant rate (the "limiting velocity"), leading to an inverse-square law to describe the decay in density with distance from the nozzle. These are the essential features of Boynton's classical model.[1] Simons[2] generalized Boynton's model by including semi-empirical expressions for the expansion of the nozzle boundary layer.

Various investigators have provided experimental verification of the Boynton–Simons models, and have presented further modifications (e.g., Ref. 3).

C. Motivation for the GP-B plume experiment

In the experiments mentioned, typical thrust levels would be from 1 to 10 N, with mass flow rates from 1 to 10 g/s, characteristic of conventional spacecraft attitude control jets. The GP-B thrusters will generate forces which are orders of magnitude smaller ($\approx$1 mN) with correspondingly low mass flows ($\approx$1 mg/s). At these levels, the nozzle and plume flow fields are highly rarefied, leading to a breakdown of the continuum theory.

When comparing data on rarefied orifice flows, Liepmann[4] uses a Reynolds number (Re) and Knudsen number (Kn) based on the thermal velocity at stagnation, and the throat (orifice) diameter D^*,

$$\mathrm{Re}=\frac{\rho_0 D^* \sqrt{\mathcal{R} T_0}}{\mu_0}, \tag{1}$$

$$\mathrm{Kn}=\frac{\sqrt{\pi/2}}{\mathrm{Re}}. \tag{2}$$

Liepmann's experiments demonstrate that the continuum theory breaks down for Knudsen numbers near 0.01 where the flow enters the near-free molecular regime. For Knudsen numbers greater than 10, the free molecular approximation is valid.

Figure 1 shows the Knudsen number versus thrust level over the operating range of the GP-B thruster. The flow is characterized as near-free molecular over much of the range, invalidating the continuum theory for describing the plume. There are no known analytical solutions for near-

 0734-2101/92/042642-08$01.00

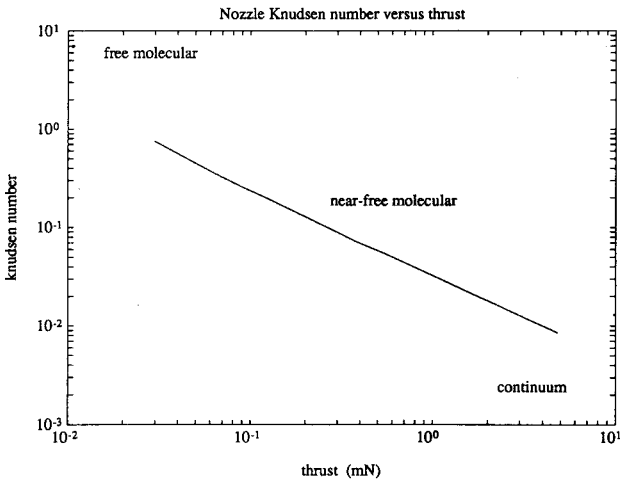

FIG. 1. Nozzle Knudsen number vs thrust.

free molecular flows, and numerical techniques such as Bird's Direct Simulation Monte Carlo (DSMC) method[5] are commonly used.

Various investigators have performed DSMC calculations on rarefied plumes and some have found excellent agreement with experiment (Refs. 6, 7, for example). However, these studies are typically limited to the near-field of the plume (within millimeters from the nozzle exit), and pertain to considerably less-rarefied flows than appropriate for the GP-B thruster.

An experiment was devised to measure the far-field mass flux variations across the plume from the GP-B thruster, using a mass spectrometer from a helium leak detector. A mass spectrometer was the instrument of choice, based on the extremely low level of flux to be measured, and on availability and cost.

II. MASS SPECTROMETER PLUME MEASUREMENTS

A. Plume experiment hardware

The mass spectrometer, from a commercially available helium leak detector (Varian 925-40), was fitted with an inlet probe, and mounted on a robotic cradle in front of the thruster (Figs. 2–4). The experiment was contained in a large vacuum chamber located at the Lockheed Santa Cruz Facility (SCF) in the Santa Cruz mountains, California. The chamber was equipped with two 32 in. diam oil diffusion pumps with a combined pumping capacity of 66 000 ℓ/s (standard, air). The pumps could maintain a background pressure between 10^{-6} and 10^{-5} Torr at the desired flow rates. The large physical dimensions of the vacuum chamber (16 ft diameter) served to diminish interference between the plume and reflected particles. The remotely controlled motorized robotic cradle could move along a horizontal circular arc, to provide measurements of the angular mass flux distributions. Motion beyond 90° from the plume centerline would position the probe behind the thruster body, enabling a *background* measurement to be made. A motorized lead screw arrangement provided radial motion of the probe. An overhead video camera provided visual input to the operator, who could control the angular position to within about one degree. Fore and aft position control was obtained by timing the motion, and comparing with a calibration curve.

The mass flow through the thruster was monitored using an MKS 1258C thermal mass flow meter, and could be varied by adjusting the stagnation pressure. The meter had a quoted range of 0–2000 sccm, with a resolution of 2 sccm, and an absolute accuracy of 16 sccm.

The thruster consisted of a plenum and a nozzle, with a restrictor upstream for additional flow control. The thruster, built by Lockheed,[8] was based on the prototypical designs of Bull[9] and Chen.[10] The nozzle area ratio was 4:1, with a half-angle 20° and a throat diameter of 2.5 mm (Fig. 1).

B. Flux measurement with the mass spectrometer

The quoted sensitivity for the Varian 125-40 leak detector is 6×10^{-9} sccm (1.8×10^{-11} mg/s).[11] This figure *does not* correspond to the sensitivity of mass flow measurement in the plume, because the leak detection relies on a different mode of operation of the mass spectrometer than the plume measurement. To understand how the mass spectrometer can be used to measure the local mass flux in the plume, requires application of some basic results from kinetic theory.

Assuming that the plume consists of a single-species Maxwellian gas, and that the instrument inlet orifice is small enough that the flow can be characterized as free molecular, then the number of particles entering the orifice per second is given by the well known result[12]

$$N_{\text{in}}=\frac{A}{2\sqrt{\pi}}n_p\xi_p\chi(S_\theta), \tag{3}$$

where

$$S=\frac{u_p}{\xi_p}, \tag{4}$$

$$S_\theta=S\sin\theta, \tag{5}$$

$$\xi=\sqrt{\frac{2kT}{m}}=\sqrt{2\mathscr{R}T}, \tag{6}$$

$$\chi(x)=e^{-x^2}+\sqrt{\pi}x[1+\operatorname{erf}(x)], \tag{7}$$

$$\operatorname{erf}(x)=\frac{2}{\sqrt{\pi}}\int_0^x e^{-\lambda^2}\,d\lambda. \tag{8}$$

S is the *speed ratio* of the plume gas, ξ is the *most probable* speed of a Maxwellian gas, and n represents number density. The c subscript pertains to the spectrometer cavity, and the p subscript pertains to the plume. A is the orifice area, and θ is the local incidence angle between the flow and the orifice. Dividing Eq. (3) by the cavity volume, $\mathscr{V}$, gives the rate of increase of number density in the cavity due to the incident stream

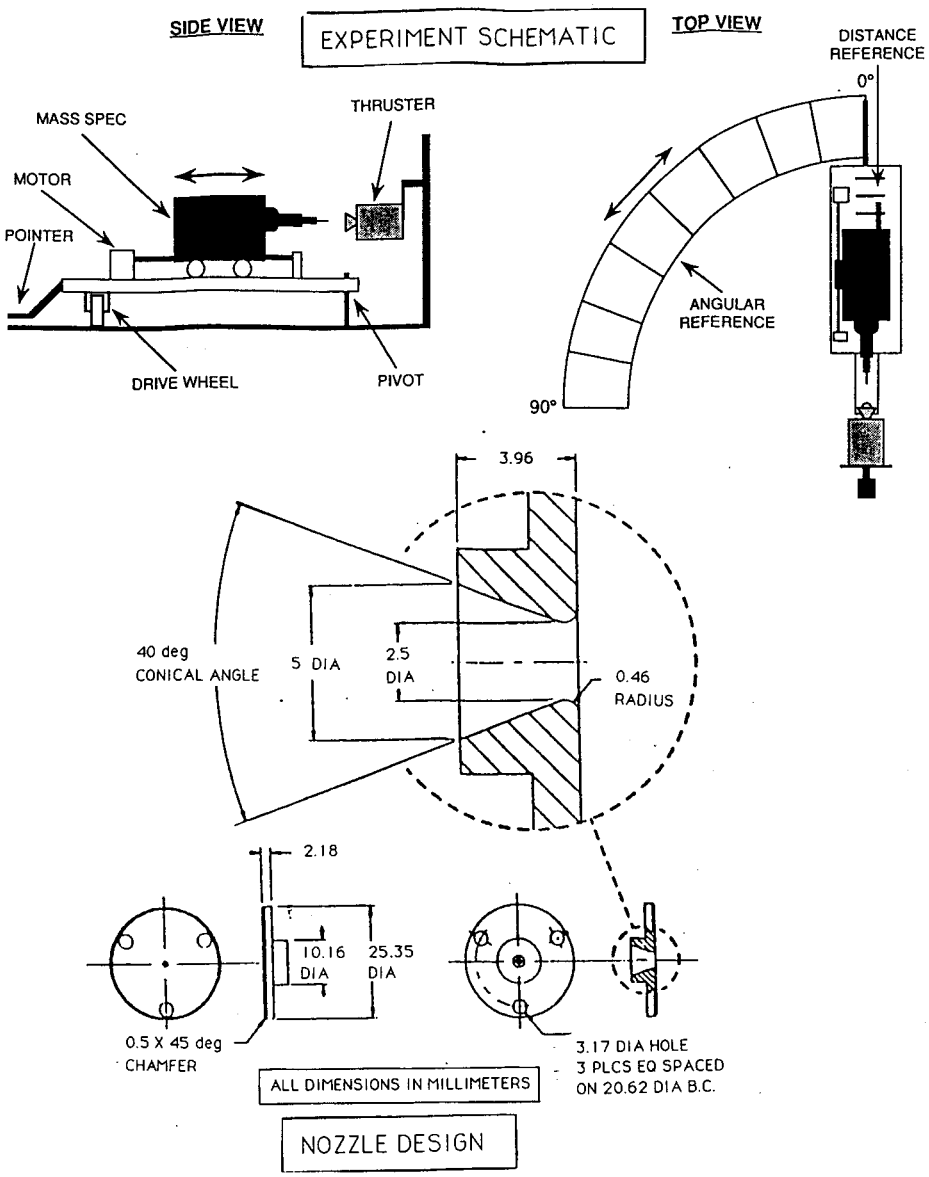

FIG. 2. Experiment schematic and nozzle geometry.

$$\left.\frac{dn_c}{dt}\right|_{\text{in}} = \frac{N_i}{\mathscr{V}} = \frac{A}{2\sqrt{\pi}\mathscr{V}} n_p \xi_p \chi(S_\theta). \tag{9}$$

Similarly, the particle flux out of the cavity is given by

$$N_{\text{out}} = \frac{A}{2\sqrt{\pi}} n_c \xi_c \chi(0) = \frac{A}{2\sqrt{\pi}} n_c \xi_c. \tag{10}$$

The argument of χ is zero here because the bulk velocity of the thermalized cavity particles is zero. The rate of decrease of number density in the cavity, due to the escaping thermalized gas is thus

$$\left.\frac{dn_c}{dt}\right|_{\text{out}} = -\frac{N_0}{\mathscr{V}} = -\frac{A}{2\sqrt{\pi}\mathscr{V}} n_c \xi_c. \tag{11}$$

The free molecular flow assumption requires that the incoming and exiting flows pass through each other without collision, in addition to the influx and efflux themselves being collisionless flows. Summing the fluxes from Eqs. (9) and (11) yields the differential equation governing the growth of density in the cavity

$$\frac{dn_c}{dt} = \frac{A}{2\sqrt{\pi}\mathscr{V}} [n_p \xi_p \chi(S_\theta) - n_c \xi_c]. \tag{12}$$

Additional terms could be included to account for the effects of adsorption and desorption, but these should be relatively insignificant for an inert gas such as helium.

In steady state, the influx balances the efflux, and Eq. (12) reduces to

$$\frac{n_c}{n_p} = \left(\frac{T_p}{T_c}\right)^{1/2} \chi(S_\theta). \tag{13}$$

A considerably simpler expression results from the fact that the speed ratio will typically be greater than unity. The velocity in the far field (>2 cm from the exit plane) is about 1300 m/s, based on the observed specific impulse of 137.[8,9] Using an average plume temperature of 100 K, Eq. (4) yields a speed ratio of 2.3. Assuming that the orifice can be oriented normal to the local flow direction at any point in the plume, then θ equals $\pi/2$, and Eq. (7) reduces to using the fact that $\text{erf}(x) \approx 1$ for $x \geqslant 1.5$

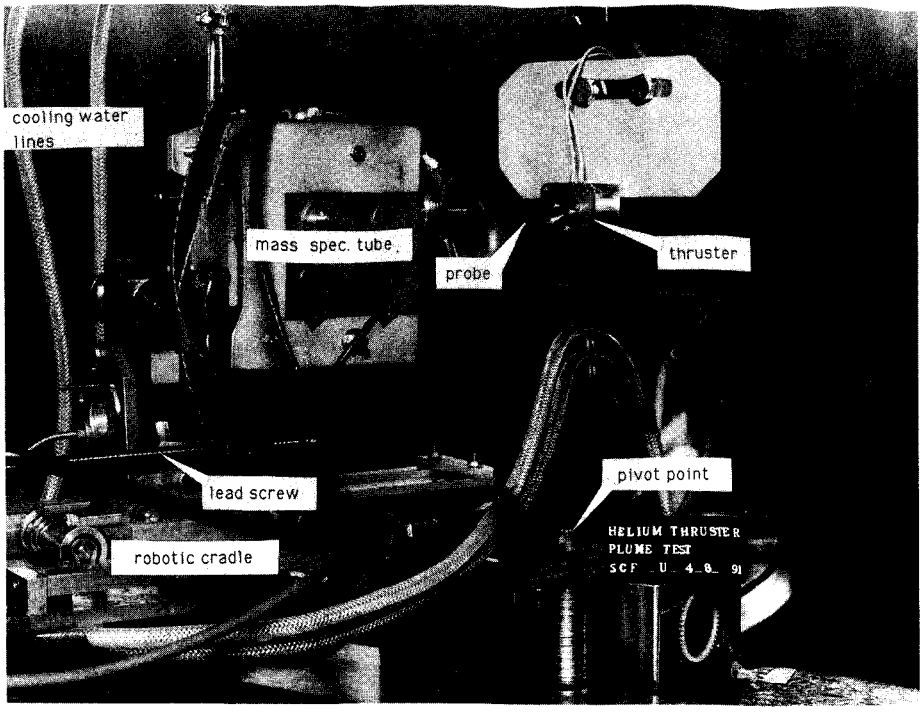

FIG. 3. The mass spectrometer tube.

$$\chi(S)\approx 2\sqrt{\pi}S. \tag{14}$$

Equation (13) reduces to

$$\frac{n_c}{n_p}=2\sqrt{\pi}\frac{u_p}{\xi_c}. \tag{15}$$

Rearranging, and noting that $\rho_p=mn_p$, then

$$\rho_p=\text{mass flux}=\frac{\xi_c}{2\sqrt{\pi}}mn_c, \quad (\text{kg m}^{-2}\,\text{s}^{-1}) \tag{16}$$

Whence, the spectrometer readout which is proportional to the density in the cavity, is directly proportional to the mass flux in the plume.

C. Correcting for the probe

The preceding analysis assumes that the entrance to the spectrometer cavity is an idealized orifice. In reality, the inlet consists of a probe, and the consequences of this merit some attention. The probe, visible in Figs. 2 and 3, consists of a cascade of copper "reducers." It was assembled to favor the incoming flow—each reducer slotted into the next largest, such that the end walls at each interconnection faced away from the incoming flow.

In order to represent the effect of the probe on the equilibrium condition, we can introduce the *Clausing coefficients*, α_i and α_0, such that the equilibrium condition becomes

$$\frac{n_c}{n_p}=\left(\frac{\alpha_i A_i}{\alpha_0 A_0}\right)\chi(S_\theta)\left(\frac{T_p}{T_c}\right)^{1/2}, \tag{17}$$

where A_i and A_0 are effective inlet and outlet areas, respectively. This differs from the original expression [Eq. (13)] by the factor $(\alpha_i A_i/\alpha_0 A_0)$. Assuming that this factor is independent of the incident velocity, it need not be known explicitly. It will be absorbed in the overall scale factor to be determined from calibration.

D. Experiment design

1. Sizing

To avoid spectrometer saturation, and to minimize the effect of interaction with ambient particles, the experiment was configured to position the probe from between 2 and 14 cm from the nozzle exit plane.

The probe inlet orifice was sized to ensure free molecular flow in both directions. The predicted mean free paths of the plume gas and the cavity gas were approximately 9 and 2 cm, respectively. Whence, to ensure that $D/\lambda \ll 1/10$, an internal diameter of 1 mm was selected for the tip of the probe.

2. Time constants

Equation (12) is a first order, linear differential equation with a straightforward solution

$$n_c(t)=2\sqrt{\pi}\frac{u_p}{\xi_c}n_p\left[1-\exp\left(-\frac{A\xi_c}{2\sqrt{\pi}\mathscr{V}}t\right)\right] \tag{18}$$

assuming a zero initial condition, and making the high speed-ratio approximation. Whence, the time constant is

$$\tau=\frac{2\sqrt{\pi}\mathscr{V}}{A\xi_c}. \tag{19}$$

Modeling the cavity as consisting of a cylindrical tube (the probe plus the inner ducting) with a 1.3 cm base radius and 10 cm length, plus three cylindrical chambers with base radii 1.5 cm and depths of 4.5 cm, then the volume is

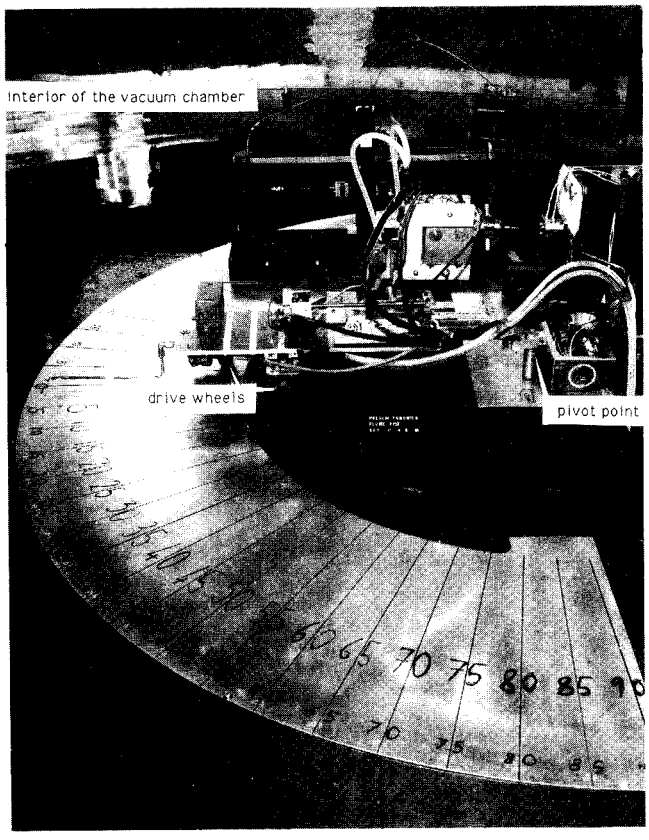

FIG. 4. Experiment hardware configuration.

approximately 1.5×10^{-4} m^3. With the 1 mm inlet diameter and a stagnation temperature of 300 K, the time constant is 0.5 s.

The effect of the probe was neglected in the preceding calculation. The time constant associated with the probe can be estimated by treating the cascade of reducers as a single "long tube" (in free molecular flow theory, a long tube is one where $\lambda \gg l \gg a$; where λ is the mean free path, l is the tube length, and a the tube radius. In this case, the requirements are not strictly met since the mean free path in the cavity is of the same order of magnitude as the tube length). Only the efflux need be considered since it is dominant. Whence, the *conductance*, F, defined as the rate of molecular flow divided by the difference in density at the ends of the tube, is given by[13]

$$F=\frac{4}{3}\frac{a^3}{l}\sqrt{2\pi\mathscr{R}T} \tag{20}$$

which has a value of 10^{-5} m^3/s for a tube length of 3 cm, tube diameter of 1 mm, and a stagnation temperature of 300 K. The differential equation governing the efflux is

$$\dot{n}_c=-\frac{F}{\mathscr{V}}(n_c-n_a) \tag{21}$$

where n_a is the chamber ambient density. Whence, the time constant is

$$\tau=\frac{\mathscr{V}}{F} \tag{22}$$

which has a value of about 15 s.

E. Tuning and calibration

1. Tuning

Having pumped the chamber down (typically overnight), coarse tuning of the mass spectrometer was performed in rough accordance with the guidelines in the leak detector instruction manual,[11] using plume gas in place of a calibrated leak. This called for adjusting the voltages until the readout attained a maximum value. It was readily apparent that even at low flow rates, there was too much helium entering the spectrometer for normal operation, and it was necessary to adjust to reduced sensitivity.

Fine tuning was essentially a process of trial and error. The control voltages were adjusted from the coarse settings until the peak readout became steady. The tuning process could take a few hours, and had to be repeated almost every day of data gathering. Extraneous events such as power fluctuations due to weather, and changes in the ambient temperature, would be enough to knock the tuning out.

2. Calibration

The mass spectrometer was calibrated at a given distance from the nozzle by recording the readout on the plume centerline for various mass flows.

By tuning the instrument to give a peak reading on the center line, there was an available dynamic range of 10^3 for characterizing the plume. The units of the readout were essentially arbitrary since an absolute calibration from readout to mass flux was not possible without an independent measure of mass flux. However, absolute calibration was not necessary for characterizing the plume structure since we were concerned only with the relative change in flux from point to point across the plume.

Early attempts at calibration were plagued by drifting scale-factors which could change by a factor of four in an hour. With the help of a thermocouple, the drift was linked to the temperature of the spectrometer tube. In a leak detector, the spectrometer tube is exposed to atmospheric conditions, and clamped to the diffusion pump, both of which serve to dissipate the heat generated by the electron filament. However, in the present mode of operation, inside the vacuum chamber, there was effectively no convective cooling from the rarefied atmosphere, and almost no conduction path through the rubber wheels of the robotic cradle. Consequently, the spectrometer body would heat up at about 1 °C/min.

To combat this problem, a length of copper tubing was bent into shape to fit snugly against the spectrometer tube body. Water at room temperature was pumped through the pipe. This simple heat exchanger was completely effective—providing passive temperature control to within 0.1 °C over an experiment sequence. Figure 5 shows some typical calibration data taken with the heat exchanger in operation.

The data follows an "S curve" with a sizeable linear region. This is encouraging because it confirms the linear-

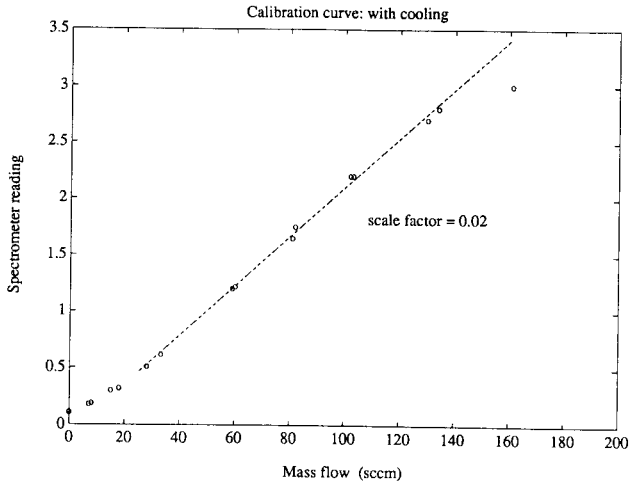

FIG. 5. Typical calibration data.

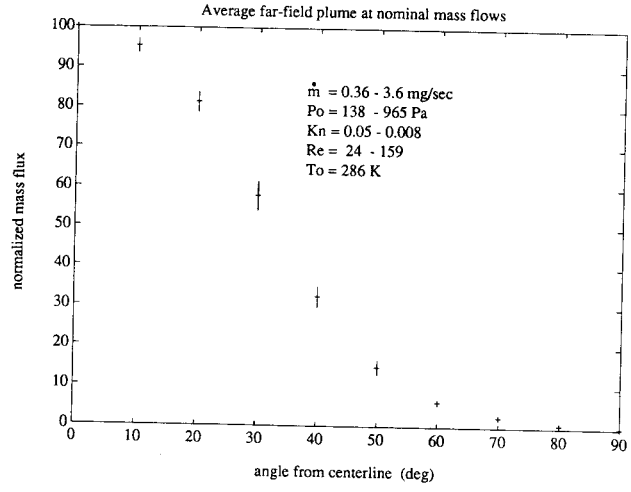

FIG. 6. Nominal far-field plume shape.

ity predicted from theory [Eq. (16)], and allows the plume shape to be characterized from the raw data in a straightforward manner.

III. RESULTS AND DISCUSSION

Plume scans were performed from the background (beyond 90°) towards the center line, in nominal intervals of 10°. The time required to reach equilibrium was about 30 s, in reasonable agreement with the predictions. Each scan was performed twice, yielding repeatability to within 5%, averaged over the scan.

Scans were performed over the mass flow range from 4 to 1200 sccm (0.01–3.6 mg/s) and at three distinct radial locations, namely 2.38, 9.25, and 13.73 cm from the nozzle exit plane. The mass flows correspond to Knudsen numbers [Eq. (2)] ranging from 1.1 to 0.01, Reynolds numbers [Eq. (1)] ranging from 1 to 160, and thrust forces ranging from 0.02 to 4.5 mN. In all cases, the background reading was the same as the reading at 90°, signifying the limit of sensitivity, and prohibiting investigation of the backflow region.

A. Far-field plume shape at nominal mass flows

The results reveal that within the bounds of experimental error, the plume shapes are the same for mass flows ranging from 14 sccm (0.04 mg/s, Kn = 0.32) to 250 sccm (0.75 mg/s, Kn = 0.03) over the range of distances from 2.38 to 13.73 cm from the nozzle exit.

The average plume shape, compiled from this data, is plotted in Fig. 6. The vertical bars represent the standard deviation from the mean, and the horizontal bars represent the one degree positioning errors.

The plot contains the normalized angular mass flux $(\rho u/\rho u|_{\phi=0})$, expressed as a percentage, obtained by subtracting the background reading, and normalizing the remainder to the centerline value.

B. Cumulative mass flux

The mass flux can be integrated over surface area to yield the cumulative mass flux which represents the fraction of the total mass flow contained within a cone of a given half-angle. For the nominal far-field plume of Fig. 6, it was found that 80% of the mass flow is contained within a 50° half-angle cone—compared with a 30° cone, typical of conventional thruster plumes.[14]

C. Plume narrowing at very low mass flows

Figure 7 reveals a distinct narrowing effect as the mass flow is decreased from 14 sccm (0.01 mg/s, Kn = 0.32), through 8 sccm (0.02 mg/s, Kn = 0.42), to 4 sccm (0.01 mg/s, Kn = 1.1). These scans were performed at the 2.38 cm radial location. The scatter in the 4 sccm data can be partly attributed to low-end loss of resolution in the mass flow meter.

This trend is supported qualitatively by the Monte Carlo results of Füstöss.[15] An intuitive supporting argu-

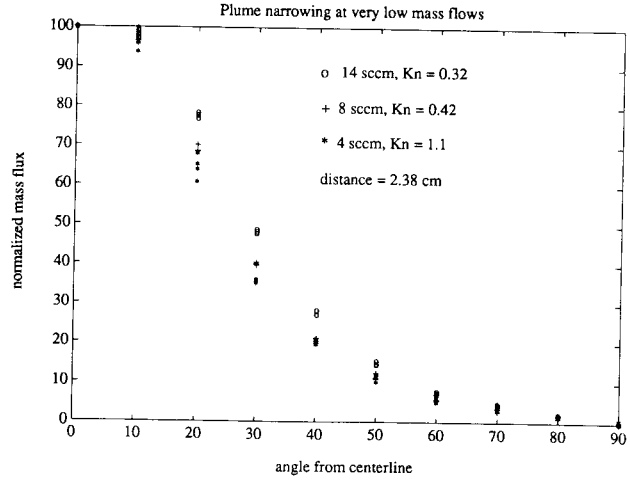

FIG. 7. Plume narrowing at very low mass flows.

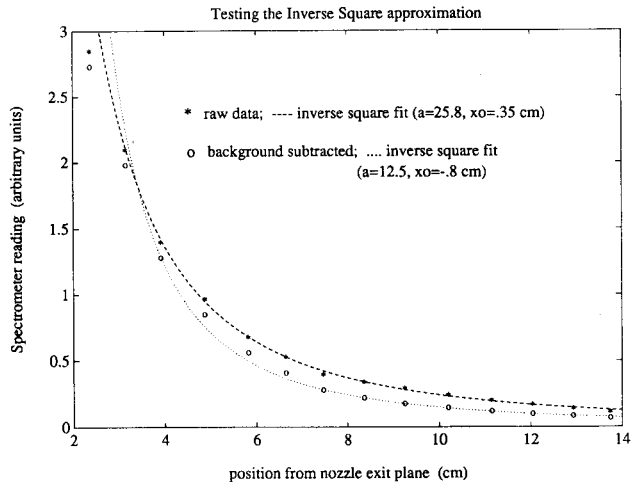

FIG. 8. Testing the inverse square model.

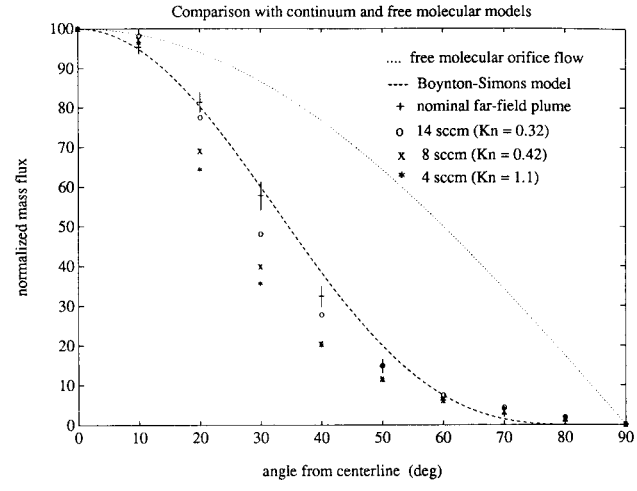

FIG. 9. Comparison with continuum and free molecular models.

ment is that the spreading due to collisions is lessened as the Knudsen number increases.

D. Limited results for high mass flows

An attempt was made to measure the plumes at the upper end of the thruster capability. Tests were performed at 600 sccm (1.8 mg/s, Kn = 0.01) and 1200 sccm (3.6 mg/s, Kn = 0.008). Owing to the problem of mass spectrometer saturation at these flow rates, data was only available outward of 35° from the centerline.

Within the bounds of experimental error, the high mass flow plumes were found to be the same as for the nominal mass flows.

E. Effect of chamber back pressure on the plume shape

In an attempt to investigate the effect of the vacuum chamber back pressure on the plume, scans were performed with one of the diffusion pumps inactive. The absence of one pump caused the chamber back pressure to double (from 8×10^{-6} to 2×10^{-5} Torr).

For this range of pressures, the effect on plume shape was found to be negligible, within the bounds of experimental error.

F. Testing for axisymmetry

One scan was performed on both sides of the plume centerline. Axisymmetry was established to within the bounds of experimental error.

G. Testing the inverse square model

Measurements were made of spectrometer reading on the center line versus probe distance from the nozzle exit plane. Figure 8 shows the results (with and without background subtraction) and the corresponding inverse-square curve fits. The fits are described by

$$y=\frac{a}{(x+x_0)^2}, \tag{23}$$

where a and x_0 were obtained by a least-squares computation.

The data closely follows an inverse square law. It is reasonable that the instrument data point departs from the inverse square model since there cannot really be a singularity at the origin.

The "virtual point source," given by x_0 from the fits, is located 8 mm in front of the nozzle exit plane, using the data with the background subtracted. Normalizing by the exit radius (2.5 mm) gives x_0/r_e equal to 3.2 for the data with the background removed. By comparison, Dettleff *et al.*[3] report x_0 and x_0/r_e equal to 9 mm and 3.8, respectively, for a nitrogen plume from a thruster with a Knudsen number of 6×10^{-5} [from Eq. (2)]. These are very close to our results, which is remarkable considering the large difference in flow conditions.

H. Comparison with the Boynton-Simons model

Figure 9 compares the experimental data with the Boynton–Simons (continuum) model. The model agrees remarkably well with the nominal far-field plume data, considering that the flow lies outside the continuum regime. As expected, the model fails to predict the narrowing trend at the higher Knudsen numbers.

I. Comparison with exact free molecular orifice flow

In the free molecular limit, the exit angular mass flux from a stagnation Maxwellian gas escaping through an ideal orifice is described by a pure cosine law, also shown in Fig. 9. This model significantly overestimates the width of the GP-B thruster plumes, which is reasonable, since one expects the nozzle walls to have a collimating effect.

IV. CONCLUSIONS

Far-field plume mass flux distributions have been obtained for Knudsen numbers ranging from 0.01 to 1.1. The results are unique because existing data pertains to considerably lower Knudsen numbers, and regions of the plume much closer to the nozzle exit.

It was found that the plume shapes do not vary appreciably with mass flow over the typical operational range. Nor do they change significantly with radial location, over the tested range of 2.38–13.73 cm.

This is encouraging from the aeronomic point of view, since the thrust calibration drift due to plume impingement will be limited to a few percent.

A narrowing phenomenon was observed for very low mass flows, which is qualitatively supported by Monte Carlo results from the literature.

The inverse square law is found to be a valid representation for the radial mass flux profiles of the rarefied plumes, and the isentropic core of the Boynton–Simons continuum model offers a remarkably close description of the angular flux distribution at the nominal flow rates.

The GP-B thruster plumes are generally wider than for conventional spacecraft control jets, evidenced from the cumulative mass flux results.

ACKNOWLEDGMENTS

A portion of this research was performed by the first author in partial fulfillment of the requirements for the degree of Doctor of Philosophy from the Department of Aeronautics and Astronautics, Stanford University. The authors wish to acknowledge the advice and support of Professor Dan DeBra, Stanford University. The work was supported by Gravity probe-B, W. W. Hansen Experimental Physics Laboratory, Stanford University, under NASA Contract No. NAS8-36125. The authors are also indebted to Lockheed Missiles and Space Company, with special thanks to James Barrs and Wes Lister of the Lockheed Santa Cruz Facility. Thanks also to Gerry Rooks, of Varian, for helpful suggestions.

[1]F. P. Boynton, AIAA J. **1**, 1703 (1967).
[2]G. A. Simons, AIAA J. **10**, 1534 (1972).
[3]G. Dettleff, R. D. Boettcher, C. Dankert, G. Koppenwallner, and H. Legge, J. Spacecraft Rockets **23**, 476 (1986).
[4]H. W. Liepmann, J. Fluid Mechanics **10**, 65 (1961).
[5]G. A. Bird, 12th International Symposium on Rarefied Gas Dynamics, AIAA, Charlottesville, VA, July 1980 (unpublished).
[6]D. A. Nelson and Y. C. Doo, 16th International Symposium on Rarefied Gas Dynamics, AIAA, Pasadena, CA, July 1988 (unpublished).
[7]P. F. Penko *et al.*, 27th Joint Propulsion Conference, June 1991 (unpublished).
[8]J. Vanden Beukel *et al.*, Technical Report No. LMSC/F420198, Lockheed Missiles and Space Co., Sunnyvale, CA, April 1991.
[9]J. S. Bull, PhD thesis, Stanford University, March 1973.
[10]J. H. Chen, PhD thesis, Stanford University, December 1983.
[11]Varian Vacuum Division, 121 Hartwell Avenue, Lexington, Massachusetts 02173, Varian 125 Leak Detector Instruction Manual.
[12]M. N. Kogan, *Rarefied Gas Dynamics* (Plenum, New York, 1969).
[13]Handbook of Vacuum Physics, edited by A. H. Beck (Pergamon, New York, 1966), Vol. 1, parts 4–6.
[14]J. C. Lengrand, 14th International Symposium on Rarefied Gas Dynamics, Tsukuba Science City, Japan, 1984 (unpublished).
[15]L. Fustoss, Vacuum **37**, 75 (1987).